ADVANCED ENGINEERING MATERIALS

DOI: 10.1002/adem.200600192

Coaxial Nanorods of MgO Core with Si Shell Layers

By *Hyoun Woo Kim** and *Seung Hyun Shim*

The current trend towards downsized integrated electronic and optical devices has strongly motivated intensive study of various one-dimensional (1D) nanostructures. An important issue of current research in 1D nanostructures is how to rationally control the size, shape, and geometrical arrangement of these nanostructures in order to produce specific properties towards desired functions in nanodevices.[1] In particular, the multilayered coaxial 1D nanostructures with core-shell geometry may realize various tailor-made functions by assembling different features of both nanowires (as cores) and nanotubes (as shells) with different chemical compositions in the radial direction.[2] Accordingly, many different coaxial nanostructures have been synthesized by a large number of research groups. Indeed, they have already demonstrated the great potential in nanodevice applications such as coaxial-gated transistors and laser diodes.[3–5] In addition, the insulating shell layer can protect nanowire cores from contamination or oxidation.[6–9] Accordingly, several research groups have successfully synthesized coaxial nanocable-like 1D structures comprised of different kinds of materials, such as Si/CdSe,[10] Ge/Si,[11] Ge/SiO_x,[12] Ge/C,[13] Au/TiO_2,[14] Au/SiO_x,[15] Ag/SiO_x,[16] Zn/ZnO,[17] ZnO/Al_2O_3,[18] ZnO/SiO_2,[19] SiC/SiO_x,[20] SiC/BN,[21] GaP/SiO_x,[22] GaP/GaN,[23] GaN/C,[24] CdSe/ZnS,[25] InS/SiO_2,[26] CdTe/SiO_2,[27] and CdS/SiO_x[28] core-shell structures.

In the present study, for the first time we have fabricated the MgO/Si core-shell structures, by wrapping the MgO nanowires with the Si layers. Radial heterostructure of Si on MgO was investigated to explore the potential of our approach to core-shell structures in materials of technological importance. Not only is MgO a typical wide bandgap insulator with its electronic and optical properties being well investigated,[29–31] but also with its excellent thermodynamic stability, low dielectric constant, and low refractive index, it has been widely used as a transition layer for growing various thin-film materials. Si is regarded as the most important semiconductor material, in which using Si not only offers the possibility of integration with conventional integrated circuits (IC) technology and fabrication equipment, but the Si shell will also play the key role on nano-devices, optoelectronic devices, and energy-conservation devices.[32–34] Furthermore, the silicon oxide can be naturally or intentionally formed on the surface, finding use as interconnects or other applications in nanoelectronic devices.

Several techniques including sol-gel process,[16] thermal heating,[26] solution-based method,[35] and chemical vapor deposition,[36] have been employed to obtain the core-shell structures. Since the three-dimensional geometry with respect to bundles of 1D structures requires high degree of the process control for achieving the conformal coating, it is worth developing suitable growth method. In this paper, we have performed the coating of Si by the plasma-enhanced chemical vapor deposition (PECVD) technique. In spite of their scientific and technological importance, only limited kind of coaxial nanostructure with the PECVD-grown shell such as carbon nanotubes/SiO_x core-shell structures has been obtained until now.[37] We have investigated comparatively the samples before and after the Si coating in terms of their structural and photoluminescence (PL) characteristics.

Figures 1(a) and 1(b), respectively, show typical top-view scanning electron microscopy (SEM) images of the uncoated and Si-coated MgO nanorods, indicating that both products consist of 1D structures. Statistical analysis of many SEM images indicated that the average diameter of the produced 1D structures without and with Si coating were in the range of 70–120 nm and 90–150 nm, respectively, revealing that Si coating contributed to thickening MgO nanorods. The diameter distributions of uncoated and coated nanorods are

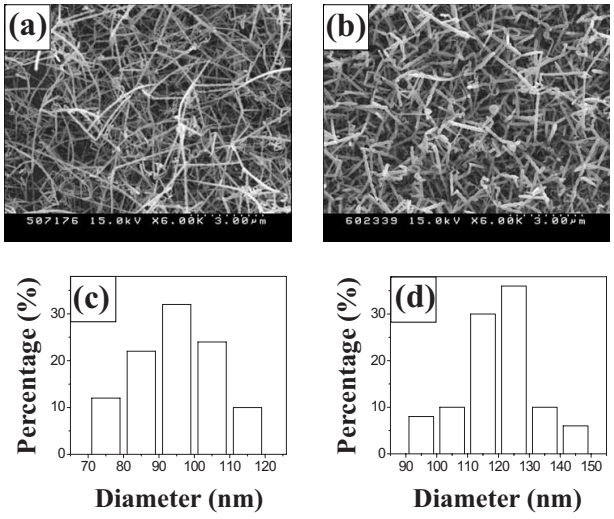

Fig. 1. Top-view SEM images of (a) uncoated and (b) coated products. The diameter distribution of (c) uncoated and (d) coated products.

[*] *Prof. H. W. Kim, S. H. Shim*
School of Materials Science and Engineering
Inha Universiy
Incheon 402-751, Korea
E-mail: hwkim@inha.ac.kr

ADVANCED ENGINEERING MATERIALS

shown in Figures 1(c) and 1(d), respectively. They reveal that the maxima of diameter distributions occur in range of 90–100 nm and 120–130 nm, respectively, for the MgO nanorods without and with the Si coating.

Figure 2(a) shows a low magnification transmission electron microscopy (TEM) image of an uncoated MgO nanorod with a straight-line morphology. The inset in Figure 2(a) gives the associated selected area electron diffraction (SAED) pattern, taken along the [001] zone axis. It can be indexed based on a cubic MgO cell with lattice parameter of a = 0.421 nm. A local high resolution TEM (HRTEM) image of an uncoated MgO nanorod (spot A in Fig. 2(a)) is shown in Figure 2(b), appearing to be structurally uniform. It is noteworthy that the surface of the nanorod is clean on an atomic scale with some steps and defects, and there is no amorphous layer covering on the surface. The resolved spacing between the parallel fringes is about 0.21 nm, corresponding to the (200) lattice plane of cubic MgO. Not only the SAED pattern but also the TEM image indicates that the MgO nanorod is crystalline.

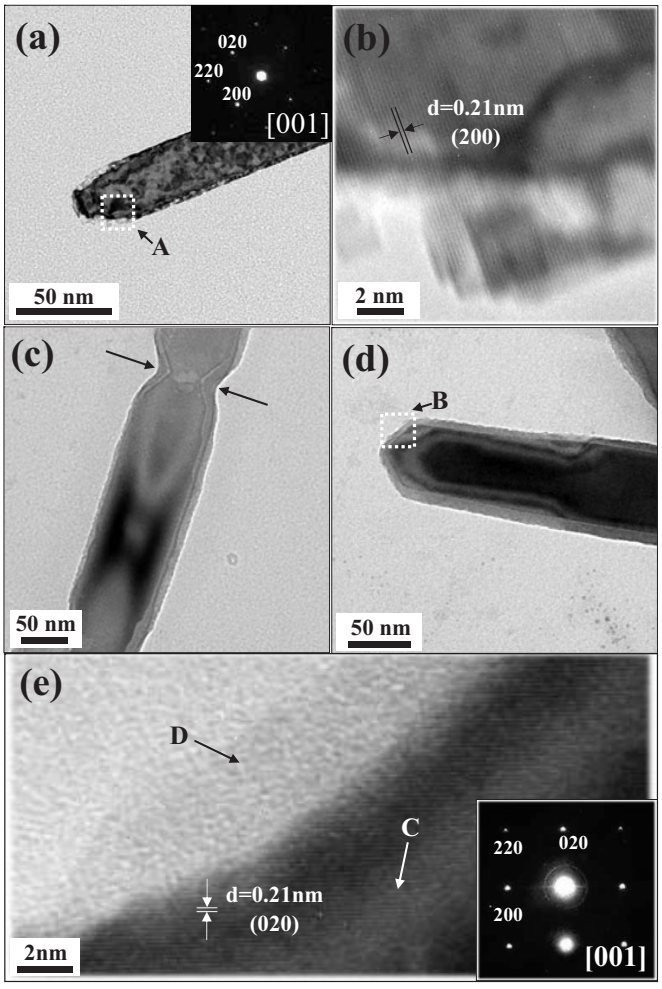

Fig. 2. (a) Low magnification TEM image of an uncoated MgO nanorod (Inset: SAED pattern of the [001] zone axis). (b) Local HRTEM image at spot A in (a). (c,d) Low magnification TEM images of coated MgO nanorods. (e) Local HRTEM image at spot B in (d) (Inset: SAED pattern of the [001] zone axis).

Figures 2(c) and 2(d) show low magnification TEM images of nanorods after Si coating, indicating that there is a layer of mist around the nanorod. A clear interface is found between the MgO core and Si shell from the TEM images. Although the thickness of the shell of individual nanorod is not perfectly uniform, the shape of the concave region can be preserved after the coating, as shown by the black arrowheads in Figure 2(c), suggesting the step-coverage characteristics of the coating process. Figure 2(e) shows a local HRTEM image corresponding to spot B in Figure 2(d). While the core of the coated structure is single crystalline evidenced by clearly visible lattice fringes (spot C in Fig. 2(e)), the shell is not single crystalline (spot D in Fig. 2(e)). The inset of Figure 2(e) shows the selected area electron diffraction (SAED) pattern of the Si-coated MgO nanorods. The SAED pattern shows a set of single-crystal electron diffraction spots corresponding to the MgO core. In addition, the pattern shows a halo presumably originating from the amorphous Si shell as well as a weak diffraction ring being consistent with Si(100), indicating that the Si shell layer is rather amorphous and contains a very small fraction of nanocrystalline region.

Figure 3(a) shows the X-ray diffraction (XRD) pattern of the coated sample. The Miller indices are indicated on each diffraction peak. The pattern exhibits the (111), (200), (220), (311), and (222) peaks of the cubic structure of MgO with a lattice constant of a=0.421 nm (JCPDS File No. 04-0829). No noticeable Si-related peaks are observed, denying the existence of single crystalline Si phase. In the XRD measurements, the angle of the incident beam to the substrate surface was approximately 0.5 °, and the detector was rotated to scan the samples. Therefore, we surmise that the peaks are mainly from the products. Energy dispersive X-ray spectroscopy

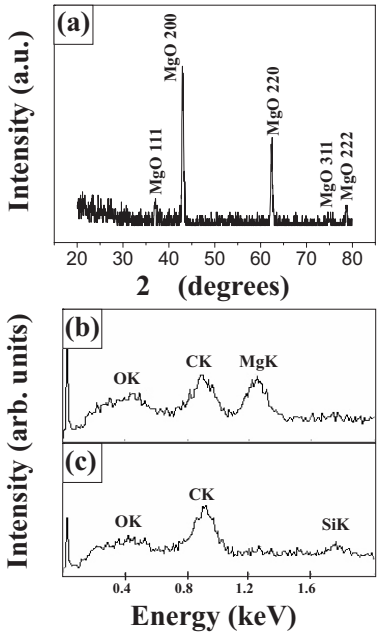

Fig. 3. (a) XRD pattern of the Si-coated MgO nanorods. EDX spectrum of the Si-coated MgO nanorods at (b) spot C and (c) spot D in (e).

(EDX) measurements made on the core region of the coated nanorods indicate that the nanorod mainly consists of Mg and O with an insignificant amount of Si (Cu signals are generated from microgrid mesh supporting the nanowires) (Fig. 3(b)). Moreover, since EDX spectrum made on the shell region (Fig. 3(c)) has a relatively higher Si/Mg atomic ratio than the spectrum obtained on the core region (Fig. 3(b)), we reveal that the outlayer comprises a Si element. Although XRD analysis does not confirm the existence of crystalline Si layer, the EDX spectrum and TEM image (including SAED pattern) suggest that the shell layer formed on the surface of the MgO nanorod core is close to amorphous Si. Also, observation from the previous experiments under the similar condition using PECVD revealed the successful deposition of Si films on flat substrates.[38,39]

There are two well-accepted mechanisms for the growth of 1D nanostructures; the vapor-liquid-solid (VLS) and the vapor-solid (VS) mechanisms. The VLS growth is a catalyst-assisted process, in which the metal catalyst particle acts as liquid-forming agent. In the present work of growing MgO nanorods, from the SEM and TEM analysis, there was no evidence that a metal-related catalyst was present at the tips of the nanorods. Hence, the growth of the MgO structure in the present route cannot be dominated by a VLS mechanism. Previous studies indicate that MgB_2 starts to decompose at ~ 800 °C,[40] and we suppose that the generated Mg vapor reacts with trace amounts of O_2 contained in this system to generate MgO in the vapor phase. The MgO nuclei precipitate on the substrate grow into MgO nanorods along with incoming of air, presumably via the VS mechanism. Subsequently, for the PECVD growth, the SiH_4 or decomposed vapor species may interact with the nanorod surface, ultimately forming the Si nuclei. It is therefore likely that the formation of Si shell layer is mainly governed by a VS process.

Figures 4(a) and 4(b) shows the PL spectra of the uncoated and coated MgO nanorods measured at room temperature. In both cases, the luminescence is mainly located in the blue region with its maximum intensity centered at around 440 nm. Gaussian fitting analysis revealed that the broad emission band was a superimposition of two major peaks, one at 432 nm in the blue region and the other at 507 nm in the blue-green region. Similar blue[41–43] and blue-green emissions[44] from MgO nanostructures have been previously observed. Both the blue and the blue-green emissions may originate from defects in MgO, such as oxygen vacancies,[45] Mg vacancies, and interstitials; presumably those defects were generated during the high-temperature evaporation process. By comparing Figure 4(b) with Figure 4(a), we found that both the intensity and the shape of PL spectrum were not noticeably changed by the Si coating. Therefore, we suggest that the amorphous Si shell layer comprising the MgO/Si core-shell structure does not significantly change the PL properties of the uncoated MgO nanorods. However, since further treatment such as thermal annealing is supposed to induce the contributory PL emissions from the Si shell layer,[38,39] the optical properties of the core-shell structure and building of advanced materials using these nanoscale blocks will be explored in future work.

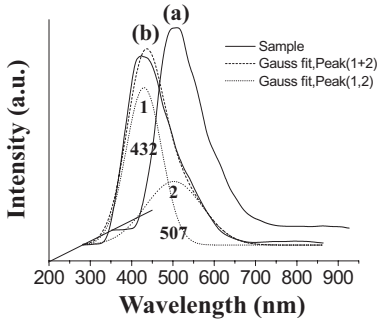

Fig. 4. (a) PL spectra of (a) uncoated and (b) coated MgO nanorods. PL spectrum in (b) exhibits the two-peak Gaussian fitting.

In summary, for the first time we have demonstrated an approach to the synthesis of MgO/Si core-shell nanorods. We have employed a PECVD technique, in which SiH_4 was used as a precursor of Si, for sheathing the MgO nanorods. Their crystallinities, morphologies and microstructures were characterized by XRD, SEM, and TEM. The Si shell was close to amorphous, whereas the MgO core was crystalline with a cubic structure. The PL of the Si-coated products under excitation at 325 nm exhibited a visible light emission, which was almost identical to that of the uncoated ones. This method can be applied to a wide range of materials and results in various Si-sheathed heterostructures, which may serve as potential building blocks in various nanodevices.

Experimental

The synthesis of the core-shell structures were carried out by a two-step process. First, we prepared the MgO nanorods by thermal evaporation of pure MgB_2 powders. The synthesis process was carried out in a quartz tube.[46] The alumina boat was put in the middle of a quartz tube inserted in a horizontal tube furnace. On top of the alumina boat containing the MgB_2 powders, a piece of the substrate was placed with the gold-coated side downwards. The furnace temperature was raised to 900 °C and was held for 2 h under a constant flow of carrier gas consisting of 97 % Ar and 3 % O_2 with a total pressure of 2 Torr. After the reaction, the substrate was cooled down and then transferred to a plasma enhanced chemical vapor deposition (PECVD) chamber.

Subsequently, we have carried out the coating experiments on the as-grown MgO nanorods by the PECVD technique, using a mixture of SiH_4 and Ar gas. The flow rates of SiH_4 and Ar gases were 100 and 40 sccm, respectively. The schematic diagram of the PECVD system is shown in Figure 5. The background pressure of the chamber was set to 4.0×10^{-5} Pa. The films were deposited at room temperature for 1 h.

The structural properties of the product were characterized by glancing angle (0.5 °) X-ray diffraction (XRD) (Philips X'pert MRD diffractometer with CuKa radiation), field emission scanning electron microscopy (FE-SEM) (Hitachi, S-4200), and transmission electron microscopy (TEM) (Philips, CM-200) with a energy dispersive X-ray spectroscopy (EDX) attached. TEM sample was prepared by ultrasonically dispersing the product in acetone and subsequently transferring to a copper grid. Photoluminescence spectroscopy (PL) was conducted at room temperature with the 325 nm line from a He-Cd laser (Kimon, 1K, Japan).

Received: July 14, 2006
Final version: August 20, 2006

ADVANCED ENGINEERING MATERIALS

[1] Y. Wu, H. Yao, M. Huang, B. Messer, J. H. Song, P. Yang, *Chem. Eur. J.* **2002**, *8*, 1261.
[2] Y. Zhang, K. Suenage, C. Colliex, S. Iijima, *Science* **1998**, *281*, 973.
[3] Y. Yu, J. Xiang, C. Yang, W. Lu, C. M. Lieber, *Nature* **2004**, *450*, 61.
[4] L. J. Lauhon, M. S. Gudiksen, D. Wang, C. M. Lieber, *Nature* **2002**, *420*, 57.
[5] H.-J. Choi, J. C. Johnson, R. He, S.-K. Lee, F. Kim, P. Pauzauskie, J. Golberger, R. J. Saykally, P. Yang, *J. Phys. Chem. B* **2003**, *107*, 8721.
[6] Y. Zhang, K. Suenaga, C. Colliex, S. Iijima, *Science* **1998**, *281*, 973.
[7] S. Han, C. Li, Z. Q. Liu, B. Lei, D. H. Zhang, W. Jin, X. L. Liu, T. Tang, C. W. Zhou, *Nano Lett.* **2004**, *4*, 1241.
[8] L. J. Lauhon, M. S. Gudiksen, D. L. Wang, C. M. Lieber, *Nature* **2002**, *420*, 57.
[9] B. Min, J. S. Lee, J. W. Hwang, K. H. Keem, M. I. Kang, K. Cho, M. Y. Sung, S. Kim, M.-S. Lee, S. O. Park, J. T. Moon, *J. Cryst. Growth* **2003**, *252*, 565.
[10] Q. Li, C. Wang, *J. Am. Chem. Soc.* **2005**, *125*, 9892.
[11] L. J. Lauhon, M. S. Gudiksen, D. Wang, C. M. Lieber, *Nature* **2002**, 420, 57.
[12] X.-M. Meng, J.-Q. Hu, Y. Jiang, C.-S. Lee, S.-T. Lee, *Appl. Phys. Lett.* **2003**, *83*, 2241.
[13] Y. Wu, P. Yang, *Appl. Phys. Lett.* **2000**, *77*, 43.
[14] Y.-G. Guo, L.-J. Wan, C.-L. Bai, *J. Phys. Chem. B* **2003**, *107*, 5441.
[15] S. O. Obare, N. R. Jana, C. J. Murphy, *Nano Lett.* **2001**, *1*, 601.
[16] Y. Yin, Y. Lu, Y. Sun, Y. Xia, *Nano Lett.* 2002, *2*, 427.
[17] Y. Ding, X. Y. Kong, Z. L. Wang, *J. Appl. Phys.* **2004**, *95*, 306.
[18] J. Hwang, B. Min, J. S. Lee, K. Keem, K. Cho, M.-Y. Sung, M.-S. Lee, S. Kim, *Adv. Mater.* **2004**, *16*, 422.
[19] L. Dai, X. L. Chen, X. Zhang, T. Zhou, B. Hu, *Appl. Phys. A* **2004**, *78*, 557.
[20] G. W. Meng, L. D. Zhang, C. M. Mo, S. Y. Zhang, Y. Qin, S. P. Feng, H. J. Li, *J. Mater. Res.* **1998**, *13*, 2533.
[21] C. Tang, Y. Bando, T. Sato, K. Kurashima, *Adv. Mater.* **2002**, *14*, 1046.
[22] S. Y. Bae, H. W. Seo, H. C. Choi, D. S. Han, J. Park, *J. Phys. Chem. B* **2005**, *109*, 8496.
[23] H.-M. Lin, Y.-L. Chen, J. Yang, Y.-C. Liu, K.-M. Yin, J.-K. Kai, F.-R. Chen, L.-C. Chen, Y.-F. Chen, C.-C. Chen, *Nano Lett.* **2003**, *3*, 537.
[24] W. Han, A. Zettle, *Adv. Mater.* **2002**, *14*, 1560.
[25] T. Mokari, U. Banin, *Chem. Mater.* **2003**, *15*, 3955.
[26] Y. B. Li, Y. Bando, D. Golberg, Y. Uemura, *Appl. Phys. Lett.* **2003**, *83*, 3999.
[27] Y. Wang, Z. Tang, X. Liang, L. M. Liz-Marzan, N. A. Kotov, *Nano Lett.* **2004**, *4*, 225.
[28] A. Pan, S. Wang, R. Liu, C. Li, B. Zou, *Small* **2005**, *1*, 1058.
[29] G. P. Summers, T. M. Wilson, B. T. Jeffries, H. T. Tohver, Y. Chen, M. M. Abraham, *Phys. Rev. B* **1983**, *27*, 1283.
[30] G. H. Rosenblatt, M. W. Rowe, G. P. Williams, Jr., R. T. Williams, Y. Chen, *Phys. Rev. B* **1989**, *39*, 10309.
[31] J. L. Grant, R. Cooper, P. Zeglinski, J. F. Boas, *J. Chem. Phys.* **1989**, *90*, 807.
[32] A. M. Morales, C. M. Lieber, *Science* **1998**, *279*, 208.
[33] A. P. Alivisatos, *Science* **1996**, *271*, 933.
[34] Y. Zhang, Q. Zhang, N. Wang, Y. Yan, H. Zhou, J. Zhu, *J. Cryst. Growth* **2001**, *226*, 185.
[35] Y.-G. Guo, L.-J. Wan, C.-L. Bai, *J. Phys. Chem. B* **2003**, *107*, 5441.
[36] L. J. Lauhon, M. S. Gudiksen, D. Wang, C. M. Lieber, *Nature* **2002**, *420*, 57.
[37] J. Hu, Z. Wang, W. Zhang, Z. Xu, Y. Wu, Z. Zhu, X. Duan, *Carbon* **2006**, *44*, 1581.
[38] M.-B. Park, N.-H. Cho, *Appl. Surf. Sci.* **2002**, *190*, 151.
[39] J.-H. Shim, S. Im, Y. J. Kim, N.-H. Cho, *Thin Solid Films* **2006**, *503*, 55.
[40] Y. Yin, G. Zhang, Y. Xia, *Adv. Funct. Mater.* **2002**, *12*, 293.
[41] Y. Hao, G. Meng, C. Ye, X. Zhang, L. Zhang, *J. Phys. Chem. B* **2005**, 109, 11204.
[42] F. L. Deepak, P. Saldanha, S. R. C. Vivekchand, A. Govindaraj, *Chem. Phys. Lett.* **2006**, *417*, 535.
[43] K. P. Kalyanikutty, F. L. Deepak, C. Edem, A. Govindaraj, C. N. R. Rao, *Mater. Res. Bull.* **2005**, *40*, 831.
[44] J. Zhang, L. Zhang, *Chem. Phys. Lett.* **2002**, *363*, 293.
[45] G. H. Rosenblatt. M. W. Rowe, G. P. Williams, Jr., R. T. Williams, Y. Chen, *Phys. Rev. B* **1989**, *39*, 10309.
[46] H. W. Kim, N. H. Kim, J. H. Myung, S. H. Shim, *Phys. Stat. Sol. (a)* **2005**, *202*, 1758.

